^{68}Ga-DOTA-E[c(RGDfK)]$_2$ PET Imaging of SHARPIN-Regulated Integrin Activity in Mice

Riikka Siitonen[1], Emilia Peuhu[2,3], Anu Autio[1], Heidi Liljenbäck[1,4], Elina Mattila[2], Olli Metsälä[1], Meeri Käkelä[1], Tiina Saanijoki[1], Ingrid Dijkgraaf[5], Sirpa Jalkanen[6], Johanna Ivaska[2,7], and Anne Roivainen[1,4,8]

[1]*Turku PET Centre, University of Turku, Turku, Finland;* [2]*Turku Centre for Biotechnology, University of Turku and Åbo Akademi University, Turku, Finland;* [3]*FICAN West Cancer Research Laboratory, University of Turku and Turku University Hospital, Turku, Finland;* [4]*Turku Center for Disease Modeling, University of Turku, Turku, Finland;* [5]*Department of Biochemistry, University of Maastricht, Maastricht, the Netherlands;* [6]*MediCity Research Laboratory, University of Turku, Turku, Finland;* [7]*Department of Biochemistry, University of Turku, Turku, Finland; and* [8]*Turku PET Centre, Turku University Hospital, Turku, Finland*

Shank-associated RH domain-interacting protein (SHARPIN) is a cytosolic protein that plays a key role in activation of nuclear factor κ-light-chain enhancer of activated B cells and regulation of inflammation. Furthermore, SHARPIN controls integrin-dependent cell adhesion and migration in several normal and malignant cell types, and loss of SHARPIN correlates with increased integrin activity in mice. Arginyl-glycyl-aspartic acid (RGD), a cell adhesion tripeptide motif, is an integrin recognition sequence that facilitates PET imaging of integrin upregulation during tumor angiogenesis. We hypothesized that increased integrin activity due to loss of SHARPIN protein would affect the uptake of $\alpha_v\beta_3$-selective cyclic, dimeric peptide ^{68}Ga-DOTA-E[c(RGDfK)]$_2$, where E[c(RGDfk)]$_2$ = glutamic acid-[cyclo(arginyl-glycyl-aspartic acid-D-phenylalanine-lysine)], both in several tissue types and in the tumor microenvironment. To test this hypothesis, we used RGD-based in vivo PET imaging to evaluate wild-type (wt) and SHARPIN-deficient mice (*Sharpin^cpdm*, where cpdm = chronic proliferative dermatitis in mice) with and without melanoma tumor allografts. **Methods:** *Sharpin^cpdm* mice with spontaneous null mutation in the *Sharpin* gene and their wt littermates with or without B16-F10-luc melanoma tumors were studied by in vivo imaging and ex vivo measurements with cyclic-RGD peptide ^{68}Ga-DOTA-E[c(RGDfK)]$_2$. After the last ^{68}Ga-DOTA-E[c(RGDfK)]$_2$ peptide PET/CT, tumors were cut into cryosections for autoradiography, histology, and immunohistochemistry. **Results:** The ex vivo uptake of ^{68}Ga-DOTA-E[c(RGDfK)]$_2$ in the mouse skin and tumor was significantly higher in *Sharpin^cpdm* mice than in wt mice. B16-F10-luc tumors were detected 4 d after inoculation, without differences in volume or blood flow between the mouse strains. PET imaging with ^{68}Ga-DOTA-E[c(RGDfK)]$_2$ peptide at day 10 after inoculation revealed significantly higher uptake in the tumors transplanted into *Sharpin^cpdm* mice than in wt mice. Furthermore, tumor vascularization was increased in the *Sharpin^cpdm* mice. **Conclusion:** *Sharpin^cpdm* mice demonstrated increased integrin activity and vascularization in B16-F10-luc melanoma tumors, as demonstrated by RGD-based in vivo PET imaging. These data indicate that SHARPIN, a protein previously associated with increased cancer growth and metastasis, may also have important regulatory roles in controlling the tumor microenvironment.

Tumor growth depends on the acquisition of new vasculature, which in turn contributes significantly to the occurrence of metastasis in distant organs. Invasion and migration of endothelial cells in response to vascular endothelial growth factor signaling and integrin-mediated cell adhesion are central to the angiogenic process (*1*). Integrins are heterodimeric transmembrane receptors consisting of an α- and a β-subunit that bind to extracellular matrix proteins and mediate signals from the cell exterior to cytoplasm and vice versa (*2*). In particular, $\alpha_v\beta_3$ integrin, which recognizes the cyclic arginyl-glycyl-aspartic acid (cRGD) tripeptide motif with high affinity, is upregulated in angiogenic endothelial cells (*3*). Even though several integrin recognize RGD motifs, RGD peptides and analogs can be engineered to be integrin heterodimer–selective. Here, we have exploited a highly $\alpha_v\beta_3$-selective radiolabeled [c(RGDfK)]$_2$ dimeric peptide to visualize alterations in $\alpha_v\beta_3$ integrin ligand binding such as may occur during tumor angiogenesis (*4*).

Molecular imaging of $\alpha_v\beta_3$ integrin expression provides information on the tumor vasculature because of its high expression on angiogenic endothelial cells, which are absent from most intact normal tissue. $\alpha_v\beta_3$ integrin binds to the 3-amino-acid sequence RGD present in different extracellular matrix proteins such as fibronectin and vitronectin (*1*). Numerous compounds based on the RGD amino acid sequence have been designed to antagonize the function of $\alpha_v\beta_3$ integrin, and cyclization of RGD peptides enhances the receptor-binding affinity and selectivity to $\alpha_v\beta_3$ integrin. The recently developed ^{68}Ga-labeled [c(RGDfK)]$_2$ dimeric peptide ^{68}Ga-DOTA-E[c(RGDfK)]$_2$, where E[c(RGDfk)]$_2$ = glutamic acid-[cyclo(arginyl-glycyl-aspartic acid-D-phenylalanine-lysine)], has a higher binding affinity to $\alpha_v\beta_3$ than does the ^{68}Ga-DOTA-E-c(RGDfK) monomer (half-maximal inhibitory concentration, 9.0 vs. 24 nM). Moreover, the dimeric [c(RGDfK)]$_2$ has shown better tumor uptake than the monomeric analog (*5*). It has been previously determined that cyclic, multimeric RGD peptides provide a useful tool for PET imaging of $\alpha_v\beta_3$ integrin expression not only

in tumor models but also in models where the tumor vasculature expresses only $\alpha_v\beta_3$ integrin (6).

Cancer-related inflammation is a well-recognized feature that contributes to the development and progression of tumors (7). Vascular adhesion protein 1 (VAP-1) is an endothelial adhesion molecule that supports trafficking of immune cells to sites of inflammation. VAP-1 contributes to tumor angiogenesis by increasing the recruitment of myeloid leukocytes into the tumor (8). We previously showed that sialic acid–binding immunoglobulin-like lectin 9 (Siglec-9) is a VAP-1 ligand and that labeled Siglec-9 motif–containing peptide can be used for PET imaging of inflammation and B16 melanoma tumors (9).

Shank-associated RH domain-interacting protein (SHARPIN) is a multifunctional protein previously implicated in nuclear factor κ-light-chain enhancer of activated B-cell activation and regulation of inflammation, as well as in the promotion of tumor growth and metastasis (10,11). SHARPIN also functions as an endogenous integrin inhibitor that binds to intracellular integrin α-tails and inhibits binding of activators to the β-subunit (12). SHARPIN-deficient mice (*Sharpin*^{cpdm}, where cpdm = chronic proliferative dermatitis in mice) with a spontaneous null mutation exhibit progressive multiorgan inflammation with a chronic eosinophilic hyperproliferative dermatitis phenotype that starts at 3–5 wk of age (13,14), which means that we limit the lifespan of the mice to 7 wk of age (Fig. 1A). In these mice, increased integrin activity has been detected in the skin, leukocytes, and mammary gland stromal fibroblasts (12,15–17). Although integrins are known to play an important role in tumor

growth, invasion, angiogenesis, and metastasis (1), it is currently unclear how regulation of integrin activity in the tumor microenvironment influences these processes. Furthermore, whether SHARPIN expression in surrounding tissue plays a role in tumor growth or metastasis has not previously been addressed experimentally. Here, we examined how SHARPIN deficiency affects cRGDfK dimeric peptide biodistribution in mice with or without melanoma tumor allografts. In addition, the role of stromal SHARPIN in regulation of tumor growth, metastasis, and vascularization was investigated. VAP-1–targeted ^{68}Ga-DOTA-Siglec-9 was used to evaluate tumor-associated inflammation in B16 melanoma tumors.

MATERIALS AND METHODS

Animals

The National Animal Experiment Board in Finland and the Regional State Administrative Agency for Southern Finland approved the animal experiments (license numbers ESAVI/3116/04.10.07/2017 and ESAVI/9339/04.10.07/2016). The experiments were conducted in accordance with the European Union directive relating to the conduct of animal experimentation. The animals were housed in standard conditions with water and food available ad libitum. Male and female mice harboring a spontaneous null mutation in the *Sharpin* gene (C57BL/KaLawRij-*SHARPIN*^{cpdm}/RiJSunJ, strain 007599, Jackson Laboratory; abbreviated *Sharpin*^{cpdm}) and littermate wild-type (wt) mice (13,14) were studied with or without B16-F10-luc (B16) melanoma tumor allografts grown between the ages of 5–7 wk.
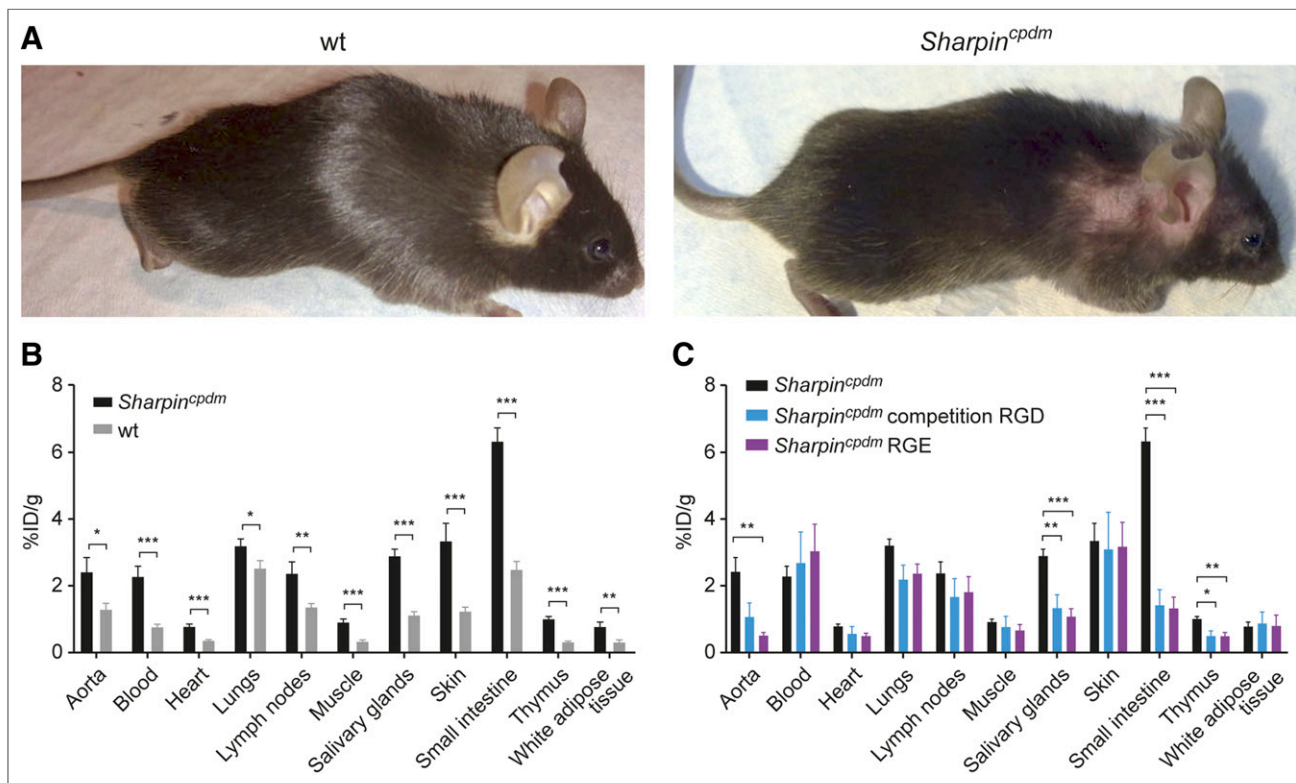

FIGURE 1. Increased tissue uptake of ^{68}Ga-DOTA-E[c(RGDfK)]$_2$ in *Sharpin*^{cpdm} mice. (A) Alopecia on dorsal skin of *Sharpin*^{cpdm} mouse, with wt littermate for comparison. (B) Ex vivo uptake of ^{68}Ga-DOTA-E[c(RGDfK)]$_2$ in *Sharpin*^{cpdm} and wt mice without tumors. (C) Competition with nonlabeled DOTA-E[c(RGDfK)]$_2$ peptide and imaging with control peptide ^{68}Ga-DOTA-E[c(RGEfK)]$_2$ revealing specific binding of tracer. Ex vivo results are expressed as percentage of injected radioactivity dose per gram of tissue (%ID/g). n = 4–9/group. *P < 0.05. **P < 0.01. ***P < 0.001.

B16 Melanoma Footpad Tumor Model

B16 murine melanoma cells (B16-F10-luc-2G5) were cultured in modified Eagle medium (MEM) supplemented with 10% fetal calf serum, MEM vitamin solution (Gibco; Invitrogen), L-glutamine, sodium pyruvate, and penicillin-streptomycin (Sigma-Aldrich). The right hind leg footpads of wt and *Sharpin^cpdm* mice were sterilized with alcohol, tumor cells were mixed with Matrigel, and the cell suspension (1×10^6 per animal in 20 μL) was immediately injected into the right hind leg. The growth of the tumor was followed for 14 d. After 14 d, the mice were killed, the primary tumor was weighed, and any metastasis to adjacent popliteal lymph nodes was explored.

B16 Melanoma Model and Experimental Design

B16 murine melanoma cells (B16-F10-luc-2G5) were cultured in MEM supplemented with 10% fetal calf serum, MEM vitamin solution (Gibco; Invitrogen), L-glutamine, sodium pyruvate, and penicillin–streptomycin (Sigma-Aldrich). *Sharpin^cpdm* ($n = 12$; weight, 20 ± 2.5 g) and wt ($n = 12$; weight, 22 ± 2.0 g) mice at the age of 5.5 wk were subcutaneously injected with B16 melanoma cells (1×10^6 per animal in 100 μL) into the neck area.

One day after inoculation, the growth of B16 melanoma cells was verified by bioluminescence imaging (IVIS Spectrum; Perkin Elmer). Furthermore, the growth of the melanoma tumors was monitored on days 1, 4, 6, 7, 8, and 9 after inoculation by ultrasound imaging (Vevo2100; VisualSonics). Nontargeted contrast agent–enhanced ultrasound (Micro-Marker; VisualSonics) was performed 9 d after inoculation to measure blood flow in the tumors. After 7, 9, and 10 d after inoculation, PET/CT was performed with ^{68}Ga-DOTA-E[c(RGDfK)]$_2$. ^{68}Ga-DOTA-Siglec-9 PET imaging was performed on a subset of mice on days 7 and 9 after inoculation. B16 melanoma tumor–bearing mice were killed after the last ^{68}Ga-DOTA-E[c(RGDfK)]$_2$ PET/CT exam, and uptake of ^{68}Ga-DOTA-E[c(RGDfK)]$_2$ was evaluated by ex vivo γ-counting and autoradiography.

Ultrasound Imaging

In brief, B16 tumor–bearing mice were anesthetized with isoflurane and positioned on a heated platform, and a solid-state MS250 transducer was placed on the tumor. Tumor sizes were measured with ultrasound (Vevo 2100; VisualSonics) at the indicated days after B16 melanoma inoculation. Tumor volumes were calculated using the formula $V = \pi/6 \times (shortest\ diameter)^2 \times (longest\ diameter)^2$.

To measure blood flow in tumors, the tail vein was cannulated with a 27-gauge catheter for intravenous administration of the contrast agent (Vevo MicroMarker; VisualSonics). The nontargeted contrast agent consists of phospholipid shell microbubbles filled with nitrogen and perfluorobutane. A 50-μL bolus (5×10^7 microbubbles) injection was delivered via the tail vein catheter.

Regions of interest were manually defined around the entire tumor area to determine how the contrast agent infiltrated the tumor over time. To measure blood flow in the tumor, a region of the graph was selected where the initial rise was observed and where the plateau was first reached. The time to peak was used as the measure of blood flow in the tumor.

Radiochemistry

^{68}Ga was obtained from a ^{68}Ga/^{68}Ge generator (Eckert and Ziegler) by elution with 0.1 M HCl. ^{68}Ga eluate (500 μL) was mixed with 2-[4-(2-hydroxyethyl)piperazin-1-yl]ethanesulfonic acid (HEPES; 120 mg) to give a pH of approximately 4.1.

For ^{68}Ga labeling, 5 μg of DOTA-E[c(RGDfK)]$_2$ (3 nmol, dissolved in deionized water) was added to the mixture, and it was heated at 100°C for 15 min. Radiochemical purity of ^{68}Ga-DOTA-E[c(RGDfK)]$_2$ was determined by reversed-phase high-performance liquid chromatography coupled with a radiodetector (Jupiter C18, 4.6×150 mm, 300 Å, 5 μm; Phenomenex). The high-performance liquid chromatography conditions were as follows: flow rate = 1 mL/min; λ = 220 nm; A = 0.1% trifluoroacetic acid/H$_2$O; B = 0.1% trifluoroacetic acid/acetonitrile. The A/B gradient was as follows: 0–2 min, 82/18; 2–11 min, from 82/18 to 40/60; 11–14 min, 40/60; 14–15 min, from 40/60 to 82/18; and 15–20 min, 82/18.

The control peptide precursor, DOTA-E[c(RGEfK)]$_2$, where E[c(RGEfk)]$_2$ = glutamic acid-[cyclo(arginyl-glycyl-glutamic acid-D-phenylalanine-lysine)], was purchased from Peptides International. For ^{68}Ga labeling, 5 μg of DOTA-E[c(RGEfK)]$_2$ (3 nmol, dissolved in deionized water) was added to the ^{68}Ga eluate and HEPES mixture and heated at 100°C for 15 min. Radiochemical purity of ^{68}Ga-DOTA-E[c(RGEfK)]$_2$ was determined as described above. ^{68}Ga-DOTA-Siglec-9 was synthesized as previously described (*18*).

PET/CT Studies

To study the biodistribution of ^{68}Ga-DOTA-E[c(RGDfK)]$_2$, *Sharpin^cpdm* ($n = 7$; weight, 20 ± 1.3 g) and wt ($n = 9$; weight, 20 ± 2.8 g) mice were imaged in vivo with an Inveon Multimodality PET/CT scanner (Siemens Medical Solutions) before ex vivo biodistribution studies. The mice were injected with ^{68}Ga-DOTA-E[c(RGDfK)]$_2$ (10 ± 1.0 MBq) via a tail vein, and a 30-min dynamic PET scan was performed. The PET data were acquired in list mode and iteratively reconstructed with an ordered-subset expectation maximization 2-dimensional algorithm into 6×10, 4×60, and 5×300 s time frames. In *Sharpin^cpdm* mice, the specificity of ^{68}Ga-DOTA-E[c(RGDfK)]$_2$ uptake was verified by competitive studies with an 18 mg/kg dose of nonlabeled DOTA-E[c(RGDfK)]$_2$ ($n = 4$/group) and imaging with the control peptide ^{68}Ga-DOTA-E[c(RGEfK)]$_2$ (9.1 ± 0.60 MBq; $n = 5$/group).

After PET/CT, animals were sacrificed, samples of the skin and other selected tissues were excised and weighed, and radioactivity was measured using a γ-counter (Triathler 3″; Hidex). The results are expressed as percentage of injected radioactivity dose per gram of tissue.

Seven, 9, and 10 d after B16 melanoma inoculation, mice were anesthetized with isoflurane and cannulated via the tail vein. They were intravenously injected with ^{68}Ga-DOTA-E[c(RGDfK)]$_2$ (9.6 ± 2.3 MBq) or ^{68}Ga-DOTA-Siglec-9 (5.5 ± 0.72 MBq) through the tail vein catheter, and 60-min ^{68}Ga-DOTA-E[c(RGDfK)]$_2$ and 30-min ^{68}Ga-DOTA-Siglec-9 PET acquisitions were performed before ex vivo and autoradiography studies. The PET data were reconstructed with an ordered-subset expectation maximization 3-dimensional algorithm followed by maximum a posteriori reconstruction into 8×30, 6×60, and 10×300 s time frames for ^{68}Ga-DOTA-E[c(RGDfK)]$_2$ and 6×10, 4×60, and 5×300 s time frames for ^{68}Ga-DOTA-Siglec-9. Quantitative PET analysis was performed by defining the tumor region of interest using Carimas 2.9 software (Turku PET Centre). Tracer accumulation was expressed as SUVs.

During the last PET/CT acquisition, the mice were intravenously administered anti-VAP-1 monoclonal antibody (clone 7–88; 1 mg/kg) 10 min before being killed (*19*). Mice were then killed, and the radioactivity of excised tissues was expressed as SUV, as determined by a γ-counter. For autoradiography, the excised tumor was frozen, cut into 20- and 8-μm cryosections, and apposed to an imaging plate. After the exposure time, the plates were scanned with a Fuji Analyzer BAS-5000 (internal resolution, 25 μm). Regions of interest were defined in tumor, tumor border, periphery of tumor, and skin, in accordance with the hematoxylin–eosin staining. Tina 2.1 software (Raytest Isopenmessgeräte) was used to measure the average ^{68}Ga-DOTA-E[c(RGDfK)]$_2$ accumulation for several tissue sections of each mouse as photostimulated luminescence per square millimeter. The background count was subtracted from the image data, and the results were normalized for injected radioactivity dose, animal weight, and radioactivity decay.
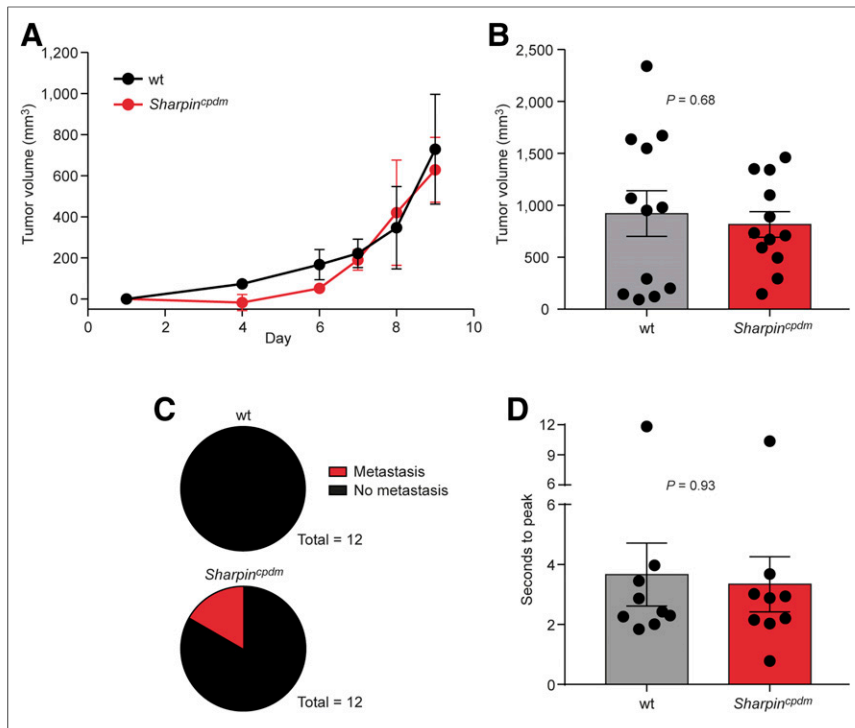
FIGURE 2. SHARPIN deficiency increases metastasis but not growth in tumor microenvironment. (A) Growth curves of B16 melanoma tumors during follow-up period (n = 8–9/group). (B) Tumor volume at end of experiment in wt and *Sharpin^cpdm* mice. (C) Pie-chart presenting lymph node metastasis (red) vs. no metastasis (black) in B16 melanoma tumor–bearing wt and *Sharpin^cpdm* mice. (D) Quantification of blood flow in B16 melanoma tumors.

Histology and Immunofluorescence

Tumor cryosections (20 μm) were stained with hematoxylin–eosin and scanned with a digital slide scanner (Panoramic 250 Flash; 3DHistech). The morphology of each tumor section was examined using Panoramic Viewer, version 1.15 software (3DHistech). To study vascularization, β_3 integrin expression, and invasion of inflammatory cells, tumor cryosections (8 μm) were immunolabeled with CD31, β_3 integrin, or CD45 primary antibodies and fluorochrome-conjugated secondary antibodies. For detection of luminal VAP-1, the sections were stained with secondary antirat immunoglobulin (Supplemental Table 1; supplemental materials are available at http://jnm.snmjournals.org).

The slides were scanned with a digital slide scanner (Panoramic Midi; 3DHistech) or an AxioVert 200M microscope (Carl Zeiss Light Microscopy) or were imaged with a 3i (Intelligent Imaging Innovations; 3i Inc) Marianas Spinning disk confocal microscope with a Yokogawa CSU-W1 scanner and Hamamatsu sCMOS Orca Flash 4.0 camera (Hamamatsu Photonics K.K.) using a ×10 objective and tile scan function. Images were analyzed using ImageJ, version 1.48 (National Institutes of Health). The percentages of positive staining for CD31, VAP-1, β3 integrin, and CD45 within the tumor area were measured using automated thresholding.

Statistical Analysis

Results are presented as mean ± SEM. Statistical analyses were performed using GraphPad Prism Software. Normality was examined using the Shapiro–Wilk test. The Student t test was used for normally distributed data, and the nonparametric Mann–Whitney U test was used for all other experiments. Comparisons between multiple groups were made using 1-way ANOVA with Tukey correction. A P value of less than 0.05 was considered significant.

RESULTS

SHARPIN Deficiency Results in Enhanced Uptake of 68Ga-DOTA-E[c(RGDfK)]₂ in Multiple Organs

The ex vivo biodistribution of ^{68}Ga-DOTA-E[c(RGDfK)]$_2$ revealed that uptake in the skin was significantly increased in *Sharpin^cpdm* mice compared with wt mice (3.3 ± 0.53 vs. 1.2 ± 0.12 percentage injected dose/g, P = 0.0006) at 30 min after injection. These data support the previously reported increase in integrin activity in the *Sharpin^cpdm* mouse epidermis (*12*). Furthermore, *Sharpin^cpdm* mice showed significantly higher ^{68}Ga-DOTA-E[c(RGDfK)]$_2$ uptake in several other tissues, including many secondary lymphoid organs (Fig. 1B).

To test if the detection was specific, we performed competitive studies with nonlabeled DOTA-E[c(RGDfK)]$_2$ peptide and imaging with the control peptide ^{68}Ga-DOTA-E[c(RGEfK)]$_2$. The excess of cold peptide could compete with the radioactive peptide binding, especially in salivary glands, small intestine, and thymus (Fig. 1C). The control peptide also provided similar results to the cold peptide.

B16 Melanoma Allografts Grow Equally in wt and Sharpin^cpdm Mice

Stromal SHARPIN deficiency had no significant effect on the growth of the B16 primary tumors at any time point during the experiments (Figs. 2A and 2B). Interestingly, lymph node metastasis was observed in 2 of 12 *Sharpin^cpdm* mice at days 9–10, whereas it was not detected in wt mice at this rather early time point (Fig. 2C). Similar results showing a subtle increase in B16 melanoma metastasis in *Sharpin^cpdm* mice were obtained when cells were injected subcutaneously into the footpad of 5-wk-old wt and *Sharpin^cpdm* mice, with higher rates of growth and metastasis to adjacent popliteal lymph nodes being observed after 14 d (11 *Sharpin^cpdm* vs. 7 wt mice had lymph node metastasis, of 16 mice of each type; Supplemental Figs. 1A and 1B). As these data are not statistically significant, it appears that SHARPIN expression in the tumor microenvironment does not significantly influence metastatic incidence in this melanoma model. The tumor perfusion rates in the B16 tumors of wt and *Sharpin^cpdm* mice at day 9 or 10 after inoculation, as measured using contrast-enhanced ultrasound imaging (Fig. 2D), were comparable, indicating that tumor vasculature may be morphologically similar between wt and *Sharpin^cpdm* mice.

In Vivo PET/CT with 68Ga-DOTA-E[c(RGDfK)]₂ Displays Increased Tracer Uptake in B16 Melanoma Allografts in Sharpin^cpdm Mice

Autoradiographs of tumor cryosections were superimposed on corresponding images of sections stained with hematoxylin–eosin, and these composite images were analyzed for accurate tracer uptake in tumor, tumor border, tumor periphery, and skin (Fig. 3A). ^{68}Ga-DOTA-E[c(RGDfK)]$_2$ autoradiographs revealed significantly increased uptake of the peptide in the skin of *Sharpin^cpdm* mice compared with wt mice (P = 0.02; Fig. 3B). In the tumor
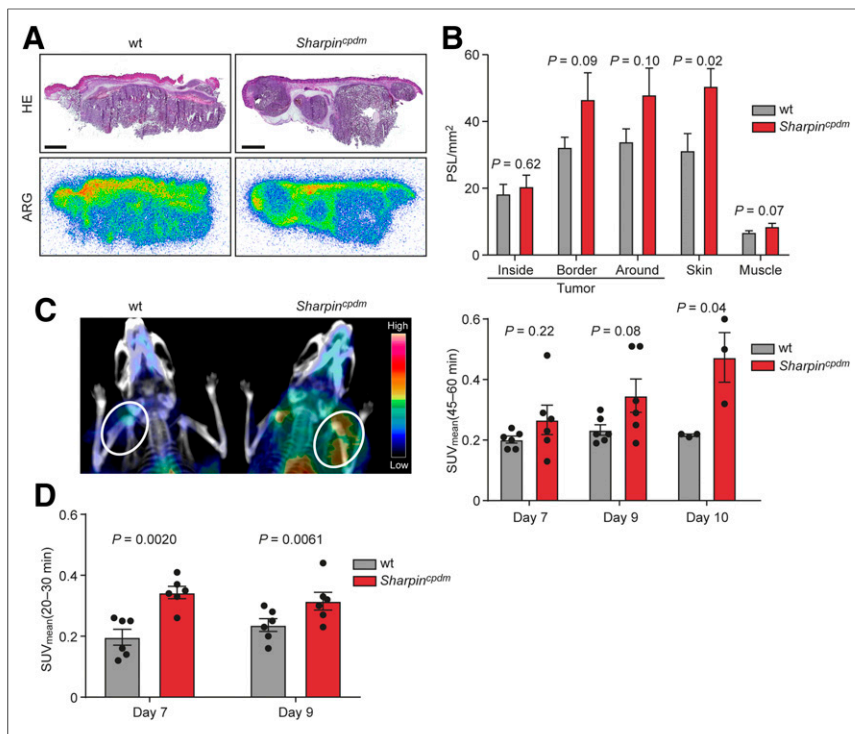
FIGURE 3. ^{68}Ga-DOTA-E[c(RGDfK)]$_2$ binding is enhanced in SHARPIN-deficient tumor microenvironment. (A) Representative autoradiographs (ARG) and corresponding hematoxylin–eosin (HE) staining of B16 melanoma tumors (scale bar, 2 mm). (B) Quantification of autoradiographs showing distribution of ^{68}Ga-DOTA-E[c(RGDfK)]$_2$ radioactivity concentration in tumor, skin, and muscle (n = 12/group). (C) Representative coronal PET/CT images of wt and *Sharpin^{cpdm}* tumor–bearing mice and in vivo tumor uptake of ^{68}Ga-DOTA-E[c(RGDfK)]$_2$ in wt and *Sharpin^{cpdm}* mice. Bars show SUV$_{mean}$ 45–60 min after injection. (D) In vivo tumor uptake of ^{68}Ga-DOTA-Siglec-9 in wt and *Sharpin^{cpdm}* mice. Bars show SUV$_{mean}$ 20–30 min after injection. PSL = photostimulated luminescence.

area, the highest radioactivity concentrations were seen in the periphery, but no significant differences in tracer uptake were detected between wt and *Sharpin^{cpdm}* tumor sections with this method (Fig. 3B). The ex vivo biodistribution at 60 min after injection showed higher ^{68}Ga-DOTA-E[c(RGDfK)]$_2$ radioactivity concentration in tumors of *Sharpin^{cpdm}* mice than in tumors of wt mice ($P < 0.05$; Table 1). Tracer uptake was markedly higher in skin and secondary lymphoid organs of *Sharpin^{cpdm}* mice (Table 1).

In vivo visualization of B16 melanoma tumors with ^{68}Ga-DOTA-E[c(RGDfK)]$_2$ was enhanced in *Sharpin^{cpdm}* mice compared with wt littermates (Fig. 3C). Importantly, the uptake of ^{68}Ga-DOTA-E[c(RGDfK)]$_2$ in the primary tumor increased in *Sharpin^{cpdm}* mice from day 7 to day 10 after inoculation (0.27 ± 0.048 vs. 0.47 ± 0.082 SUV, P = 0.048), whereas in wt mice, ^{68}Ga-DOTA-E[c(RGDfK)]$_2$ uptake did not significantly differ from day 7 to day 10 postinoculation (0.20 ± 0.011 vs. 0.22 ± 0.0033 SUV, P = 0.44). Importantly, the tumor uptake of ^{68}Ga-DOTA-E[c(RGDfK)]$_2$ at day 10 was significantly higher in *Sharpin^{cpdm}* mice than in wt littermates. The same trend was also observed at day 9 after inoculation, but the difference was not statistically significant (0.35 ± 0.055 vs. 0.23 ± 0.017 SUV, P = 0.078). An equivalent experiment was performed at days 7 and 9 after inoculation with VAP-1–targeted ^{68}Ga-DOTA-Siglec-9 to evaluate tumor-related inflammation in B16 melanoma tumors. Quantitative analysis showed

that the tumor uptake of ^{68}Ga-DOTA-Siglec-9 at both time points was significantly higher in *Sharpin^{cpdm}* mice than in wt littermates (Fig. 3D). Thus, these data indicate that tumors developing in a SHARPIN null host have higher levels of $\alpha_v\beta_3$ integrin activity and inflammation.

Stromal SHARPIN Regulates Tumor Angiogenesis

Frozen sections of B16 melanoma allografts in wt and *Sharpin^{cpdm}* mice were stained to detect luminal expression of VAP-1 on endothelial cells. Staining of luminal VAP-1, indicative of inflammation, did not show any differences between wt and *Sharpin^{cpdm}* mice (Fig. 4A). In addition, the immune cell infiltration in B16 tumors, examined by CD45 immunofluorescence staining, was similar between wt and *Sharpin^{cpdm}* mice (Supplemental Fig. 2). However, the tumors of *Sharpin^{cpdm}* mice were slightly more vascularized than those of wt mice (P = 0.04; Fig. 4B), as indicated by CD31 labeling to detect blood vessels.

β_3 integrin was expressed in tumor cells and particularly in endothelial cells of B16 melanoma allografts (Fig. 4C). The area of β_3 integrin–positive staining was more elevated in B16 melanoma allografts in *Sharpin^{cpdm}* mice than in wt mice, although the difference was not statistically significant (Fig. 4C).

DISCUSSION

Integrins play an important role during tumor progression. However, the crosstalk between integrin activity regulation and cancer is not fully understood. Therefore, this study aimed to explore the role of the integrin inactivator SHARPIN in tumor growth, invasion, angiogenesis, and metastasis. We found that, whereas primary B16 tumor size and tumor blood flow were similar in wt and *Sharpin^{cpdm}* mice, the uptake of ^{68}Ga-DOTA-E[c(RGDfK)]$_2$ in tumors was increased in *Sharpin^{cpdm}* mice. The data suggest increased $\alpha_v\beta_3$ integrin activity in *Sharpin^{cpdm}* mice. A subtle increase in the tendency of *Sharpin^{cpdm}* tumors to metastasize was also observed.

Significant increases in $\alpha_v\beta_3$ integrin radiotracer binding were observed in *Sharpin^{cpdm}* mice without B16 melanoma tumor allografts. Nonlabeled DOTA-E[c(RGDfK)]$_2$ peptide and ^{68}Ga-DOTA-E[c(RGEfK)]$_2$ peptide significantly reduced the tracer uptake in, for example, small intestine, thus indicating higher level of specific $\alpha_v\beta_3$ binding in *Sharpin^{cpdm}* mice than in the wt littermates. In competition experiments, we did not see reduced uptake in the skin of *Sharpin^{cpdm}* mice, most likely because the skin phenotype is more β_1 integrin–dependent (*15*). $\alpha_v\beta_3$ integrin is overexpressed on angiogenic endothelial cells and is a well-validated target for assessing tumor angiogenesis (*1*). However, $\alpha_v\beta_3$ integrin expression is also upregulated in chronic inflammatory

TABLE 1
Ex Vivo Biodistribution of ^{68}Ga-DOTA-E[c(RGDfK)]$_2$ in Tumor-Bearing Mice at Days 9–10 After Inoculation

Site	Sharpin[cpdm]	wt	P
Aorta	4.3 ± 0.81	2.1 ± 0.18	<0.05
Brown adipose tissue	0.92 ± 0.15	0.51 ± 0.037	<0.05
Blood	1.5 ± 0.43	0.60 ± 0.058	NS
Bone	1.4 ± 0.15	0.87 ± 0.037	<0.05
Heart	0.82 ± 0.14	0.51 ± 0.032	<0.05
Lungs	3.0 ± 0.37	2.0 ± 0.079	<0.05
Lymph nodes	2.0 ± 0.28	0.81 ± 0.056	<0.01
Muscle	0.58 ± 0.079	0.36 ± 0.016	<0.05
Skin	2.9 ± 0.41	1.3 ± 0.070	<0.01
Small intestine	5.5 ± 0.62	3.2 ± 0.39	<0.05
Thymus	1.4 ± 0.21	0.79 ± 0.041	<0.05
Tumor	1.9 ± 0.45	1.0 ± 0.15	<0.05
White adipose tissue	0.68 ± 0.16	0.43 ± 0.11	NS

Results are expressed as percentage of injected radioactivity dose per gram of tissue (mean ± SEM).

NS = not statistically significant.

processes such as in patients with rheumatoid arthritis or inflammatory bowel disease (20,21). Previous studies indicated that ^{18}F-labeled galacto-RGD and ^{64}Cu-labeled RGD tetramer reflect angiogenesis during chronic inflammation processes and can emerge as a target for molecular imaging (22,23). In line with these findings, our results further indicate that $\alpha_v\beta_3$ expression

and angiogenesis during chronic inflammation can be assessed with ^{68}Ga-DOTA-E[c(RGDfK)]$_2$ in Sharpin[cpdm] mice with multiorgan inflammation.

Previous studies indicate that SHARPIN is upregulated in human renal cell carcinoma, hepatocellular carcinoma, ovarian cancer, prostate cancer, and breast cancer (11,24–26). Additionally, SHARPIN was shown to enhance lung metastasis in an animal model of osteosarcoma (27). However, the role of SHARPIN in regulating the tumor stroma has not been investigated, albeit in the developing mammary gland it plays an essential role in regulating stromal architecture (16). In our B16 melanoma model, stromal SHARPIN had no significant effect on tumor growth or blood flow. Impaired blood flow in tumors may result from tumor vasculature that is morphologically abnormal, and many molecular differences exist between tumor and normal vasculature (1). However, angiogenesis measured by CD31 immunolabeling was increased in Sharpin[cpdm] compared with wt tumor mice. Furthermore, we showed that stromal SHARPIN might have a tendency to reduce, rather than increase, melanoma metastasis to the lymph nodes. Vascular endothelial growth factor A stimulates growth and differentiation of endothelial cells and increases their permeability. Increased permeability leads to increased migration of tumor cells through endothelium and into the bloodstream, which is a common route for metastases to form (28). Expression of vascular endothelial growth factor A messenger RNA is increased in skin lesions of Sharpin[cpdm] mice, where the number of blood vessels is increased (29). In addition, we observed that tumor uptake of VAP-1–targeting ^{68}Ga-DOTA-Siglec-9 was significantly higher in Sharpin[cpdm] than in wt mice. However, immunofluorescence staining of VAP-1–positive vessels to indicate inflammation in tumors did not differ between Sharpin[cpdm] and wt mice. This finding may be a result of weak VAP-1 expression in intratumoral vessels, which was previously reported for human melanoma (30). These findings are complementary to the concept that stromal SHARPIN regulates the angiogenesis and metastasis formation that occurs because of tortuous and leaky tumor vasculature, thus facilitating migration through impaired endothelium.

In the subcutaneous murine B16 melanoma model, we found that tumor uptake of ^{68}Ga-DOTA-E[c(RGDfK)]$_2$ was significantly increased in Sharpin[cpdm] mice at 10 d after inoculation. However, the increased uptake of RGD in Sharpin[cpdm] tumor mice cannot be explained by increased tumor perfusion or tumor size. The ligand-binding affinity of $\alpha_v\beta_3$ integrin is not constant and can be modulated by a process called inside-out signaling. Inside-out activation is caused by the binding of integrin-activating proteins such as talins and kindlins to the cytoplasmic domain of integrins, where they can change their conformation. (3) However, SHARPIN inhibits this activation switch (12). Immunofluorescence staining of B16 tumor sections showed a trend toward more positive β_3 integrin staining in
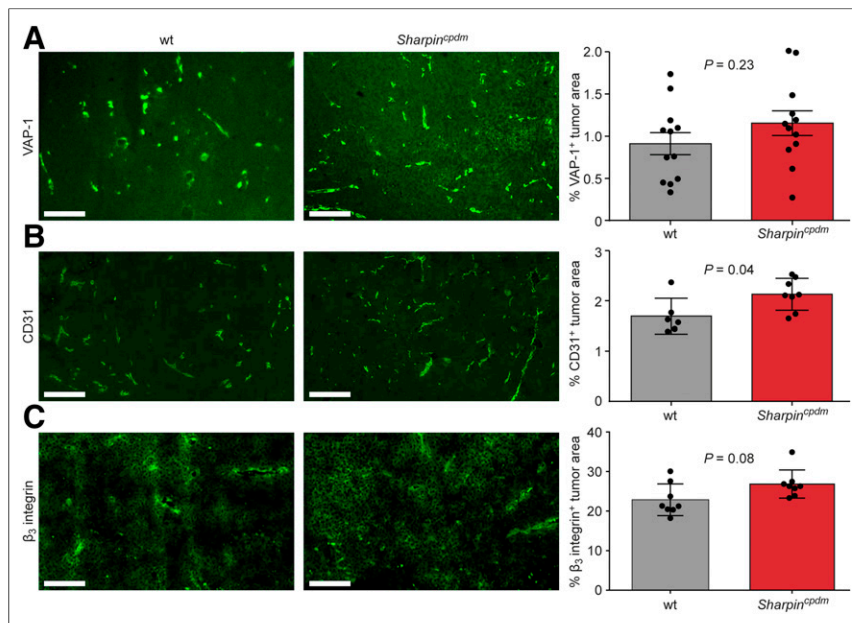

FIGURE 4. Stromal SHARPIN regulates tumor vascularization. (A–C) Representative cryosections of B16 tumors from wt and Sharpin[cpdm] mouse immunolabeled with VAP-1 (A), CD31 (B), and β_3 integrin antibody (C). Scale bar, 200 μm. Bars show VAP-1–positive, CD31-positive, and β_3 integrin–positive tumor areas from B16 tumors implanted into wt and Sharpin[cpdm] mice.

Sharpin^{cpdm} mice than in wt mice, which could also contribute to the higher $\alpha_v\beta_3$ integrin activity detected by ^{68}Ga-DOTA-E[c(RGDfK)]$_2$ binding. In the present study, other RGD-motif–recognizing integrins were not investigated. Previously, 2 xenograft studies reported changes in tumor uptake of $\alpha_v\beta_3$ integrin-binding radiotracers during drug treatment (*31,32*). In the first study, mice bearing human glioblastoma U87MG cell xenografts were treated with dasatinib. The results showed that treatment can inhibit binding of ^{64}Cu-DOTA-c(RGDfK) without affecting the expression of $\alpha_v\beta_3$ integrin. In the second study, mice bearing human epidermoid carcinoma A431 cell xenografts were treated with bevacizumab, and binding of $\alpha_v\beta_3$ radiotracer was increased, even though $\alpha_v\beta_3$ expression was decreased by half. In both studies, the authors speculated that changes in cRGD uptake could not be accounted for by altered $\alpha_v\beta_3$ expression. A recently published in vitro study showed that binding of $\alpha_v\beta_3$ radiotracers to cells affected both $\alpha_v\beta_3$ integrin activation status and expression (*33*). In line with previous studies, the data presented here indicate that SHARPIN deficiency has an effect on $\alpha_v\beta_3$ integrin activation status and that ^{68}Ga-DOTA-E[c(RGDfK)]$_2$ can be used to reflect $\alpha_v\beta_3$ integrin activation.

SHARPIN is of great interest in the field of basic medical research because it is associated with both tumorigenesis and regulation of inflammation. On the basis of the results presented herein, the use of $\alpha_v\beta_3$ integrin–targeted radiotracers can be extended to be used to investigate both the tumor vasculature and $\alpha_v\beta_3$ integrin–expressing tumor cells. In addition, this study provides valuable information on the use of $\alpha_v\beta_3$ integrin–targeted radiotracers to evaluate the response to altered integrin activity.

CONCLUSION

Our results showed that stromal SHARPIN regulates the binding of ^{68}Ga-DOTA-E[c(RGDfK)]$_2$ in both a B16 melanoma model and mice without tumor allografts. Furthermore, stromal SHARPIN regulates tumor vascularization and may counteract formation of metastasis. The present study strengthens the concept of using radiolabeled cRGD peptides to provide a tool for studying changes in $\alpha_v\beta_3$ integrin activation and not only its expression. In addition, the use of radiolabeled cRGD peptides could be expanded to study inflammatory diseases.

DISCLOSURE

ACKNOWLEDGMENTS

KEY POINTS

QUESTION: Can $\alpha_v\beta_3$ integrin–targeted PET radiotracer detect a change in the integrin activity controlled by the SHARPIN protein?

PERTINENT FINDINGS: PET imaging of SHARPIN-deficient and wild-type mice with $\alpha_v\beta_3$-selective cyclic, dimeric RGDfK peptide, ^{68}Ga-DOTA-E[c(RGDfK)]$_2$, revealed that SHARPIN regulates integrin activity and vascularization in the microenvironment of melanoma and chronic proliferative dermatitis.

IMPLICATIONS FOR PATIENT CARE: The results of this study suggest that the use of $\alpha_v\beta_3$ integrin–selective radiotracers can be expanded to investigate not only the changes of $\alpha_v\beta_3$ integrin expression status but also response to altered integrin activity in both cancer and inflammatory diseases.

REFERENCES

1. Desgrosellier JS, Cheresh DA. Integrins in cancer: biological implications and therapeutic opportunities. *Nat Rev Cancer.* 2010;10:9–22.
2. Bouvard D, Pouwels J, De Franceschi N, Ivaska J. Integrin inactivators: balancing cellular functions in vitro and in vivo. *Nat Rev Mol Cell Biol.* 2013;14:430–442.
3. Pfaff M, Tangemann K, Muller B, et al. Selective recognition of cyclic RGD peptides of NMR defined conformation by αIIbβ3, αVβ3, and α5β1 integrins. *J Biol Chem.* 1994;269:20233–20238.
4. Zannetti A, Del Vecchio S, Iommelli F, et al. Imaging of $\alpha_v\beta_3$ expression by a bifunctional chimeric RGD peptide not cross-reacting with $\alpha_v\beta_5$. *Clin Cancer Res.* 2009;15:5224–5233.
5. Dijkgraaf I, Yim C-B, Franssen GM, et al. PET imaging of αvβ3 integrin expression in tumours with ^{68}Ga-labelled mono-, di- and tetrameric RGD peptides. *Eur J Nucl Med Mol Imaging.* 2011;38:128–137.
6. Lobeek D, Franssen GM, Ma MT, et al. In vivo characterization of 4 ^{68}Ga-labeled multimeric RGD peptides to image $\alpha_v\beta_3$ integrin expression in 2 human tumor xenograft mouse models. *J Nucl Med.* 2018;59:1296–1301.
7. Diakos CI, Charles KA, McMillan DC, Clarke SJ. Cancer-related inflammation and treatment effectiveness. *Lancet Oncol.* 2014;15:e493–e503.
8. Marttila-Ichihara F, Auvinen K, Elima K, Jalkanen S, Salmi M. Vascular adhesion protein-1 enhances tumor growth by supporting recruitment of Gr-1+CD11b+ myeloid cells into tumors. *Cancer Res.* 2009;69:7875–7883.
9. Aalto K, Autio A, Kiss EA, et al. Siglec-9 is a novel leukocyte ligand for vascular adhesion protein-1 and can be used in PET imaging of inflammation and cancer. *Blood.* 2011;118:3725–3733.
10. Tokunaga F, Nakagawa T, Nakahara M, et al. SHARPIN is a component of the NF-κB-activating linear ubiquitin chain assembly complex. *Nature.* 2011;471: 633–636.
11. Jung J, Kim JM, Park B, et al. Newly identified tumor-associated role of human Sharpin. *Mol Cell Biochem.* 2010;340:161–167.
12. Rantala JK, Pouwels J, Pellinen T, et al. SHARPIN is an endogenous inhibitor of β1-integrin activation. *Nat Cell Biol.* 2011;13:1315–1324.
13. HogenEsch H, Gijbels MJ, Offerman E, van Hooft J, van Bekkum DW, Zurcher C. A spontaneous mutation characterized by chronic proliferative dermatitis in C57BL mice. *Am J Pathol.* 1993;143:972–982.
14. Seymour RE, Hasham MG, Cox GA, et al. Spontaneous mutations in the mouse Sharpin gene result in multiorgan inflammation, immune system dysregulation and dermatitis. *Genes Immun.* 2007;8:416–421.
15. Peuhu E, Salomaa SI, De Franceschi N, Potter CS, Sundberg JP, Pouwels J. Integrin beta 1 inhibition alleviates the chronic hyperproliferative dermatitis phenotype of SHARPIN-deficient mice. *PLoS One.* 2017;12:e0186628.
16. Peuhu E, Kaukonen R, Lerche M, et al. SHARPIN regulates collagen architecture and ductal outgrowth in the developing mouse mammary gland. *EMBO J.* 2017;36:165–182.
17. Pouwels J, De Franceschi N, Rantakari P, et al. SHARPIN regulates uropod detachment in migrating lymphocytes. *Cell Reports.* 2013;5:619–628.
18. Siitonen R, Pietikäinen A, Liljenbäck H, et al. Targeting of vascular adhesion protein-1 by positron emission tomography visualizes sites of inflammation in *Borrelia burgdorferi*-infected mice. *Arthritis Res Ther.* 2017;19:254.

19. Merinen M, Irjala H, Salmi M, Jaakkola I, Hänninen A, Jalkanen S. Vascular adhesion protein-1 is involved in both acute and chronic inflammation in the mouse. *Am J Pathol.* 2005;166:793–800.

20. Wilder RL. Integrin alpha V beta 3 as a target for treatment of rheumatoid arthritis and related rheumatic diseases. *Ann Rheum Dis.* 2002;61(suppl 2): ii96–ii99.

21. Danese S, Sans M, de la Motte C, et al. Angiogenesis as a novel component of inflammatory bowel disease pathogenesis. *Gastroenterology.* 2006;130:2060–2073.

22. Pichler BJ, Kneilling M, Haubner R, et al. Imaging of delayed-type hypersensitivity reaction by PET and ^{18}F-galacto-RGD. *J Nucl Med.* 2005;46:184–189.

23. Cao Q, Cai W, Li ZB, et al. PET imaging of acute and chronic inflammation in living mice. *Eur J Nucl Med Mol Imaging.* 2007;34:1832–1842.

24. He L, Ingram A, Rybak AP, Tang D. Shank-interacting protein-like 1 promotes tumorigenesis via PTEN inhibition in human tumor cells. *J Clin Invest.* 2010; 120:2094–2108.

25. Li J, Lai Y, Cao Y, et al. SHARPIN overexpression induces tumorigenesis in human prostate cancer LNCaP, DU145 and PC-3 cells via NF-κB/ERK/Akt signaling pathway. *Med Oncol.* 2015;32:444.

26. De Melo J, Tang D. Elevation of SIPL1 (SHARPIN) increases breast cancer risk. *PLoS One.* 2015;10:e0127546.

27. Tomonaga M, Hashimoto N, Tokunaga F, et al. Activation of nuclear factor-kappa B by linear ubiquitin chain assembly complex contributes to lung metastasis of osteosarcoma cells. *Int J Oncol.* 2012;40:409–417.

28. Claesson-Welsh L, Welsh M. VEGFA and tumour angiogenesis. *J Intern Med.* 2013;273:114–127.

29. HogenEsch H, Sola M, Stearns TM, Silva KA, Kennedy VE, Sundberg JP. Angiogenesis in the skin of SHARPIN-deficient mice with chronic proliferative dermatitis. *Exp Mol Pathol.* 2016;101:303–307.

30. Forster-Horváth C, Döme B, Paku S, et al. Loss of vascular adhesion protein-1 expression in intratumoral microvessels of human skin melanoma. *Melanoma Res.* 2004;14:135–140.

31. Dumont RA, Hildebrandt I, Su H, et al. Noninvasive imaging of alphaVbeta3 function as a predictor of the antimigratory and antiproliferative effects of dasatinib. *Cancer Res.* 2009;69:3173–3179.

32. Rylova SN, Barnucz E, Fani M, et al. Does imaging $\alpha_v\beta_3$ integrin expression with PET detect changes in angiogenesis during bevacizumab therapy? *J Nucl Med.* 2014;55:1878–1884.

33. Andriu A, Crockett J, Dall'Angelo S, Piras M, Zanda M, Fleming IN. Binding of $\alpha_v\beta_3$ integrin-specific radiotracers is modulated by both integrin expression level and activation status. *Mol Imaging Biol.* 2018;20:27–36.